J. Fluid Mech. (2026), *vol.* 1031, R2, doi:10.1017/jfm.2026.11352



Effect of directionality on extreme wave formation during nonlinear shoaling

Jie Zhang[1,2], **Yuxiang Ma**[2], **Jiawen Sun**[3], **Limin Huang**[1], **Michel Benoit**[4,5] **and Saulo Mendes**[6]

[1]College of Shipbuilding Engineering, Harbin Engineering University, Harbin 150001, PR China

[2]State Key Laboratory of Coastal and Offshore Engineering, Dalian University of Technology, Dalian 116023, PR China

[3]National Marine Environmental Monitoring Center, Dalian 116023, PR China

[4]EDF R&D, Laboratoire National d'Hydraulique et Environnement (LNHE), Chatou 78400, France

[5]LHSV, ENPC, Institut Polytechnique de Paris, EDF R&D, Chatou 78400, France

[6]School of Civil and Environmental Engineering, Nanyang Technological University, 50 Nanyang Ave, 639798, Republic of Singapore

Corresponding author: Limin Huang, huanglimin@hrbeu.edu.cn

(Received 24 December 2025; revised 14 February 2026; accepted 23 February 2026)

Recent studies have shown that, in coastal waters where water depth decreases significantly due to rapid bathymetric changes, the non-equilibrium dynamics (NED) substantially increases the occurrence probability of extreme (rogue) waves. Nevertheless, research on depth-induced NED has been predominantly confined to unidirectional irregular waves, while the role of directionality remains largely unexplored. The scarce studies on multidirectional waves mainly rely on numerical simulations and have yielded conflicting results. In this work, we report on an experimental investigation of wave directionality on the depth-induced non-equilibrium wave statistics. High-order statistical moments, skewness and kurtosis, are used as proxies for the non-equilibrium wave response. Our results indicate that the directional spreading has a minor effect on decreasing the maximum values of these statistical moments. In contrast, the incidence direction plays a significant role in the non-equilibrium wave response, which is attributed to the effective bottom slope.

Key words: topographic effects, surface gravity waves, nonlinear instability

1. Introduction

Rogue waves, often associated with severe disasters and casualties, were once dismissed as maritime folklore until numerous encounters with vessels and offshore platforms were

© The Author(s), 2026. Published by Cambridge University Press. This is an Open Access article, distributed under the terms of the Creative Commons Attribution-NonCommercial licence (https://creativecommons.org/licenses/by-nc/4.0/), which permits non-commercial re-use, distribution, and reproduction in any medium, provided the original article is properly cited. The written permission of Cambridge University Press or the rights holder(s) must be obtained prior to any commercial use.

https://doi.org/10.1017/jfm.2026.11352 Published online by Cambridge University Press

documented (Draper 1964; Didenkulova & Pelinovsky 2020; Didenkulova, Didenkulova & Medvedev 2023). These anomalous ocean waves (with wave height reaching 2 or 2.2 times the significant wave height, by definition) occur with unexpectedly high probability (Dysthe, Krogstad & Müller 2008; Mori *et al.* 2023; Bitner-Gregersen *et al.* 2024).

Rogue wave formation essentially results from wave energy focusing through linear or nonlinear mechanisms. Numerous hypotheses regarding these focusing processes have been proposed (Kharif, Pelinovsky & Slunyaev 2009; Onorato *et al.* 2013; Adcock & Taylor 2014; Dematteis *et al.* 2019), which can be systematically categorised based on the role of nonlinearity. Linear focusing mechanisms include dispersive focusing and spatial focusing due to bathymetric or current-induced reflection and refraction (Chien, Kao & Chuang 2002). Nonlinear focusing mechanisms encompass bound wave nonlinearity (Fedele *et al.* 2016; Knobler *et al.* 2025), modulation (Benjamin–Feir) instability (Benjamin & Feir 1967; Onorato *et al.* 2009; He *et al.* 2022; Zhai *et al.* 2025) and non-equilibrium dynamics (NED) due to significant and rapid environmental changes (Trulsen 2018).

Recently, NED has attracted considerable interest as it provides a universal explanation of rogue wave formation under rapidly varying wind, current or bathymetric conditions (Trulsen, Zeng & Gramstad 2012; Annenkov & Shrira 2015; Toffoli *et al.* 2017; Zhang *et al.* 2023; Mendes, Teutsch & Kasparian 2025), or under unrealistic initial conditions (Shemer, Sergeeva & Liberzon 2010; Tang *et al.* 2022). In particular, being relevant in coastal areas, NED induced by drastic depth reduction has been intensively investigated in both numerical (Zeng & Trulsen 2012; Gramstad *et al.* 2013; Kashima, Hirayama & Mori 2014; Viotti & Dias 2014; Zheng *et al.* 2020; Lawrence *et al.* 2021*a*; Zhang, Ma & Benoit 2024*a*,*b*,*c*) and experimental flumes (Trulsen *et al.* 2012, 2020; Bolles, Speer & Moore 2019; Zhang *et al.* 2019; Wang *et al.* 2020; Lawrence *et al.* 2021*b*; Li *et al.* 2021*a*; Samseth & Trulsen 2025), focusing on statistical distributions of free surface elevation and kinematics, evolution of statistical moments and wave forces on structures. Theoretical investigations on NED have been conducted from both stochastic (Majda, Moore & Qi 2019; Majda & Qi 2020; Mendes *et al.* 2022; Mendes & Kasparian 2023) and deterministic perspectives (Li *et al.* 2021*b*; Moss *et al.* 2025).

Research on NED in three-dimensional (3-D) cases is gaining significant momentum. Using fully nonlinear potential flow models, Lawrence, Trulsen & Gramstad (2022) and Draycott & Li (2025) investigated the interplay between long-crested waves and 2-D bathymetry (circular shoals), both of which show a significant kurtosis enhancement due to NED. With the high-order spectral method, Ducrozet & Gouin (2017) showed that directional spreading strongly suppresses rogue wave formation due to depth variation, while Tang *et al.* (2023) observed a weaker directional effect. Conversely, Lyu, Mori & Kashima (2023) showed with a 2-D depth-modified nonlinear Schrödinger equation that short-crested wave fields with a larger spreading angle may increase the occurrence probability of extreme waves. Remarkably, Mei *et al.* (2023) found through a fully nonlinear Boussinesq model that directional spread can decrease the excess kurtosis in intermediate water but also increase it in shallow water. Evidently, previous studies on NED of 3-D waves are either based on numerical simulations or have been constrained by experimental facility limitations (Tang *et al.* 2023). Contradictory conclusions indicate that the effect of the wave directionality on rogue wave formation remains unclear. To address this knowledge gap, we conduct a systematic, large-scale experimental study of NED in wave fields with varying directional spreading and incident direction. We explore how the non-equilibrium parameters, skewness and kurtosis, evolve after a rapid depth variation.

https://doi.org/10.1017/jfm.2026.11352 Published online by Cambridge University Press

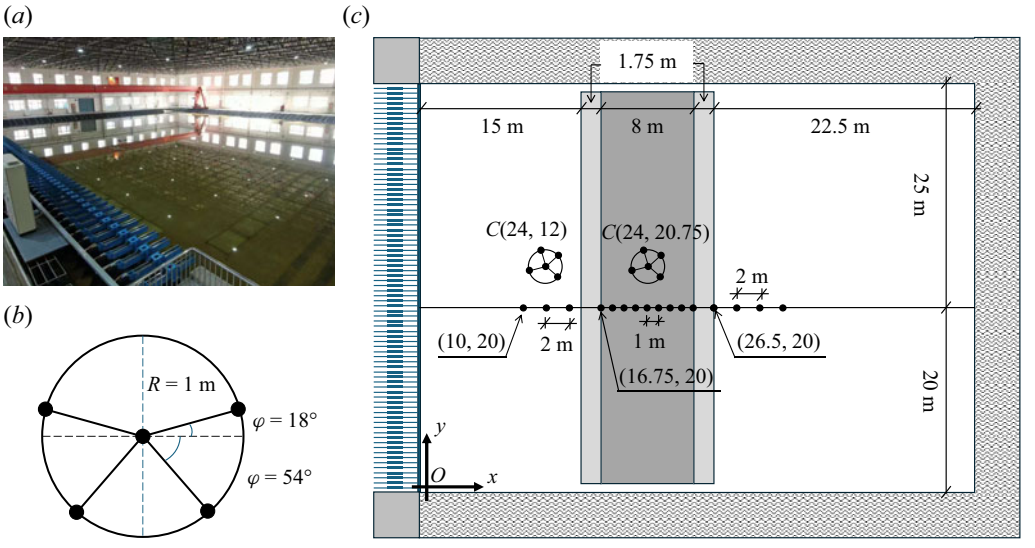


Figure 1. The NMEMC wave tank (*a*); the layout of wave gauge array following Nwogu (1989) for the estimation of directional spectrum. (*b*); the experimental wave tank and locations of the wave gauges (*c*).

2. Experimental set-up

The experimental campaign was conducted at the Multi-functional Test Basin of the National Marine Environmental Monitoring Centre (NMEMC) in Dalian, China. The wave tank is 49 m long, 47 m wide and 1.2 m deep. Waves are generated by a snake-type (consisting of 80 × 0.5 m paddles) multi-directional wavemaker installed on one shorter side of the tank. Porous medium damping zones along the opposing end and lateral boundaries are set to minimise wave reflection.

In the wave tank, an isosceles trapezoidal prism parallel to the wavemaker was installed on an otherwise flat bottom. It consists of a central flat section (8 m in width and 0.36 m in height) flanked by two transitional slopes (with a horizontal extent of 1.75 m, thus a gradient of 1/4.86). The upslope of the trapezoidal prism starts 15 m away from the wavemaker. During the experimental campaign, the water depth near the wavemaker was set to $h_1 = 0.61$ m, thus $h_2 = 0.25$ m over the submerged structure. Twenty-six resistance-type wave gauges were deployed during the tests, with a sampling frequency $f_s = 50$ Hz. Two arrays of five probes with the same configuration as introduced in Nwogu (1989) were used to estimate the directional spectra before and above the submerged bar. The remaining probes are adopted to capture the wave evolution. The schematic of the experimental basin, as well as the locations of the wave gauges, are shown in figure 1.

The wave fields are described by their directional spectrum $S(f, \theta) = S_J(f)D(\theta|f)$, with $S_J(f)$ denoting the JOint North Sea WAve Project spectrum and $D(\theta|f)$ the directional spreading function

$$S_J(f) = \frac{\alpha_J g^2}{(2\pi)^4} \frac{1}{f^5} \exp\left[-\frac{5}{4}\left(\frac{f_p}{f}\right)^4\right] \gamma^{\exp\left[-\frac{(f-f_p)^2}{2(\sigma_J f_p)^2}\right]}, \tag{2.1}$$

where g is the acceleration due to gravity, $f_p = 1/T_p$ denotes the spectral peak frequency, α_J the spectral energy parameter, γ the peakedness parameter and σ_J width parameter, $\sigma_J = 0.07$ for $f < f_p$ and $\sigma_J = 0.09$ for $f \geq f_p$. Here, the classical Mitsuyasu-type

https://doi.org/10.1017/jfm.2026.11352 Published online by Cambridge University Press

				Deeper zone ($h_1 = 0.61$ m)			Shallower zone ($h_2 = 0.25$ m)		
Case	T_p [s]	s_{max}	θ_{inc} [rad]	$H_{s,0}$ [m]	ε_0	μ_0	$H_{s,f}$ [m]	ε_f	μ_f
A1	1.6	10	0	0.032	0.021	1.165	0.033	0.031	0.671
A2		35		0.034	0.022		0.036	0.034	
A3		85		0.034	0.023		0.038	0.035	
A4		∞		0.034	0.023		0.038	0.036	
B1	2.0	10	0	0.044	0.022	0.873	0.050	0.037	0.524
B2		35	$\{0, \pi/12, \pi/6, \pi/4\}$	0.046	0.023		0.053	0.039	
B3		85	0	0.046	0.023		0.054	0.040	
B4		∞	$\{0, \pi/12, \pi/6, \pi/4\}$	0.048	0.024		0.055	0.039	

Table 1. Incident wave conditions and key non-dimensional parameters.

directional spreading function (Goda 2010) is adopted

$$D(\theta|f) = \frac{2^{2s-1}}{\pi}\frac{\Gamma^2(s+1)}{\Gamma(2s+1)}\cos^{2s}\left(\frac{\theta-\theta_{inc}}{2}\right), \tag{2.2}$$

with Γ denoting the gamma function, θ_{inc} the dominant wave direction and $s(f)$ the frequency-related angular spreading parameter, $s = s_{max}(f/f_p)^5$ for $f \le f_p$ and $s = s_{max}(f/f_p)^{-2.5}$ for $f \ge f_p$. The peak value of s, s_{max}, governs the width of the directional spreading. To avoid phase locking and ensure ergodicity of the generated wave field, we adopt the modified double summation approach for wave generation, which associates a random phase $\phi_{ij} \in [0,\ 2\pi]$ with each frequency-direction bin (f_{ij}, θ_j) (Luo *et al.* 2020)

$$\eta(y,t) = \sum_{i=2}^{N_f}\sum_{j=1}^{N_\theta} a_{ij}\cos\left(yk_{ij}\sin\theta_j - 2\pi f_{ij}t + \phi_{ij}\right), \tag{2.3}$$

where

$$\begin{cases} f_{ij} = \hat{f}_i - \dfrac{1}{2}\Delta f + \left(j - 1 + R_{ij}\right)\Delta f/N_\theta, \\ \hat{f}_i = (f_{i-1} + f_i)/2, \end{cases} \tag{2.4}$$

with N_f, N_θ denoting the discretisation points in frequency and direction, respectively, and Δf, $\Delta\theta$ being the uniform intervals. The cutoff range for the directional spectrum $S(f,\theta)$ is $f_i \in [0.5f_p,\ 3.5f_p]$ and $\theta_j \in [-\pi,\ \pi]$. Here, a_{ij}, k_{ij} and ϕ_{ij} denote the amplitude, wavenumber and random phase of the component harmonics, respectively, and R_{ij} denotes a random number in [0, 1] with a uniform probability distribution.

The configurations of incident wave fields are listed in table 1, together with non-dimensional parameters, wave steepness $\varepsilon \equiv \sqrt{2}k_p\sigma$ and relative water depth $\mu \equiv k_p h$, where σ denotes the standard deviation of the measured free surface elevation (FSE) and k_p the spectral peak wavenumber. The subscripts 0 and f denote deeper-water and shallower-water quantities, respectively. In all cases, the waves generated offshore are of relatively mild nonlinearity. Three peak periods $T_p = \{1.2,\ 1.6,\ 2.0\}$ s were examined, corresponding to weak, intermediate and strong non-equilibrium scenarios, respectively. Here, the cases with $T_p = 1.6$ and 2.0 s are shown. The peakedness parameter $\gamma = 3.3$ was maintained constant across all cases. Three directional spreading conditions $s_{max} = \{10,\ 35,\ 85\}$ were tested, in which 95 % of the integrated spectral energy of

https://doi.org/10.1017/jfm.2026.11352 Published online by Cambridge University Press

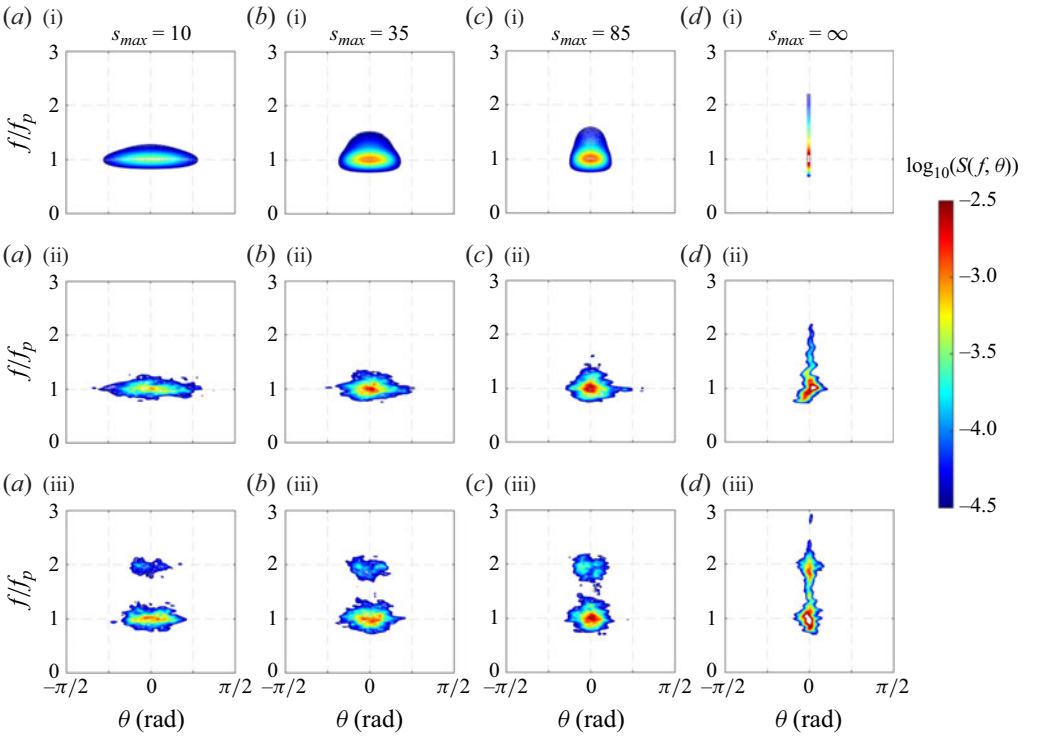


Figure 2. Target directional spectra for the normal incident cases with $s_{max} = 10$, 35, 85 and ∞ in panels (*a*.i–*b*.i); the corresponding experimental spectra measured offshore (*a*.ii–*d*.ii) and on top of the bar (*a*.iii–*d*.iii).

the total energy is concentrated within the ranges $[-0.39, 0.39]\pi$, $[-0.22, 0.22]\pi$ and $[-0.14, 0.14]\pi$, respectively. The B2 and B4 cases were tested with three oblique incidence conditions, $\theta_{inc} = \pi/12$, $\theta_{inc} = \pi/6$ and $\theta_{inc} = \pi/4$. Note that the wave gauges are shifted from $y = 20$ to $y = 24$ m in the cases with $\theta_{inc} = \pi/4$ to capture wave evolution. Each experimental run lasts 6 minutes for wave generation and data acquisition, in order to limit energy accumulation due to long-wave reflection. To ensure statistical stability, several runs with different random phase seeds were performed such that the total sample duration exceeded $5000T_p$ for each case.

3. Results and discussion

To verify the quality of directional wave field generation in the offshore area and to show the spectral evolution as waves propagate over the bar, two wave gauge arrays were deployed in the wave tank. Figure 2(*a*.i–*d*.i) shows the target spectra of the normal incidence B1–B4 cases with $\theta_{inc} = 0$ and four values of s_{max}, the corresponding spectra measured offshore (*a*.ii–*d*.ii), and on top of the bar (*a*.iii–*d*.iii). The directional estimation is achieved by using a classical iterative maximum likelihood approach. In figure 2, the measured and target spectra are in good agreement offshore, indicating that the directional wave fields were generated properly. At the top of the bar, the second-order harmonics are excited significantly after shoaling, consistent with the observations in long-crested wave scenarios. In figure 2, no evident transverse waves (propagating with $\theta \approx \pm\pi/2$) induced by sidewall reflection are present in the current colour scale, indicating the transverse waves are of amplitudes lower than those of the primary harmonics by at least two orders

https://doi.org/10.1017/jfm.2026.11352 Published online by Cambridge University Press

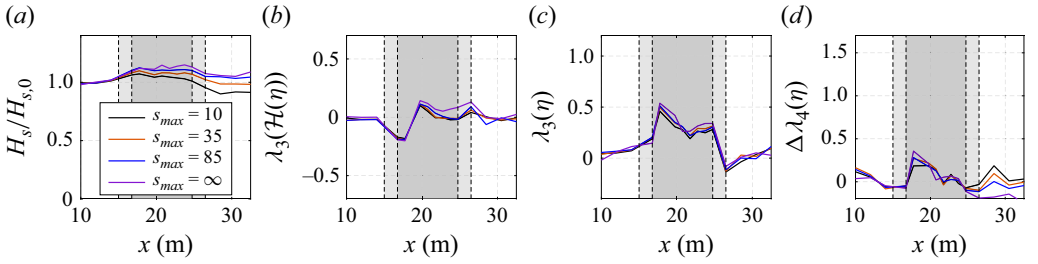


Figure 3. Spatial evolution of normalised significant wave height (*a*), asymmetry parameter (*b*), skewness (*c*) and net change of kurtosis (*d*) of cases A1–A4 (all with normal incidence, $\theta_{inc} = 0$).

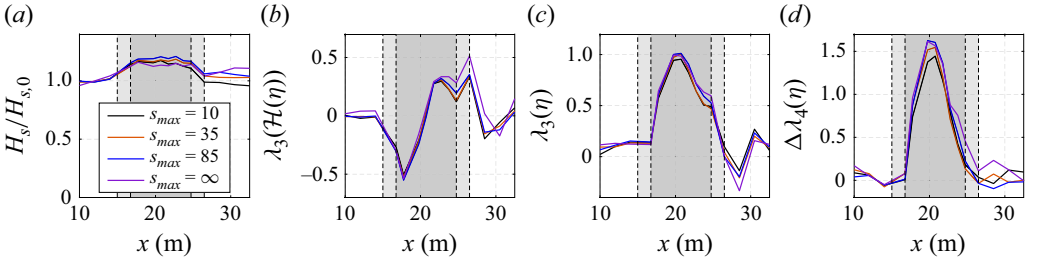


Figure 4. Same as figure 3, but for normal incident directional wave cases ($\theta_{inc} = 0$) B1–B4.

of magnitude. The wave reflection by the end wall is also small and can thus be ignored. Moreover, it is noticed that the enhancement of the second-order harmonics slightly decreases as s_{max} decreases. The same good wavemaking quality also applies to other cases with normal/oblique incidence.

Following previous works (see Onorato, Osborne & Serio 2005; Trulsen *et al.* 2020; Li *et al.* 2021*b*, for example), we focus on the evolution of third- and fourth-order statistical moments, skewness and kurtosis, of the FSE, which characterise the non-Gaussianity of sea states. Skewness, $\lambda_3(\eta) \equiv \langle(\eta - \langle\eta\rangle)^3\rangle/\sigma^3$, with $\langle\cdot\rangle$ being an averaging operator, measures the asymmetry of the wave profile in the vertical direction. Kurtosis, $\lambda_4(\eta) \equiv \langle(\eta - \langle\eta\rangle)^4\rangle/\sigma^4$, serves as a proxy of rogue wave intensity. In addition, the asymmetry parameter, $\lambda_3[\mathcal{H}(\eta)]$, measures the horizontal asymmetry of the wave profile, with $\mathcal{H}(\cdot)$ denoting Hilbert transform. In the following, the spatial evolutions of the statistical parameters are discussed, including the normalised significant wave height, asymmetry parameter, skewness and the net change of kurtosis $\Delta\lambda_4$, defined by subtracting the mean value of λ_4 prior to the shoal

$$\Delta\lambda_4(x) = \lambda_4(x) \; - \langle\lambda_4\rangle|_{0\le x\le 15\,\mathrm{m}}. \tag{3.1}$$

Using $\Delta\lambda_4$, we can isolate depth-induced effects from small influences arising from different incident sea-state conditions, thereby focusing on the relative influence of shoaling across different wave conditions.

Figure 3 shows the spatial evolution of the statistical parameters in cases A1–A4 with different directional spreadings. Figure 3(*a*) shows that the normalised significant wave height is slightly increased over the bar due to shoaling. Figures 3(*b*) and 3(*c*) indicate that the NED effects result in increased asymmetry of the mean wave profile in both horizontal and vertical directions. In figure 3(*d*), kurtosis is moderately enhanced over the bar, implying higher rogue wave probability. These observations are in line with those reported in unidirectional wave studies (see Lawrence *et al.* 2021*b*; Zhang *et al.* 2019;

https://doi.org/10.1017/jfm.2026.11352 Published online by Cambridge University Press

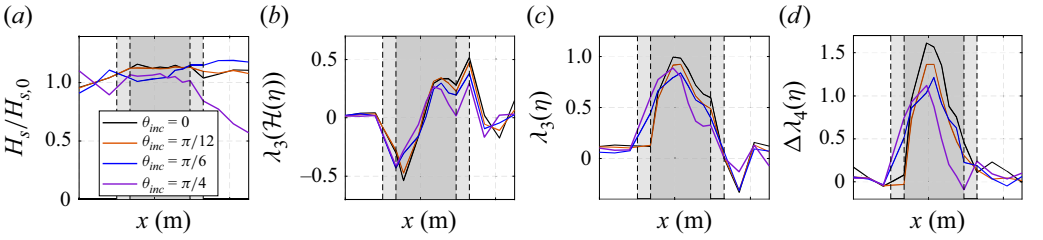


Figure 5. Same as figure 3, but for oblique incident unidirectional cases ($s_{max} = \infty$).

Zheng *et al.* 2020, for instance). Figure 4 shows the statistical parameter evolution in the normal incident B1–B4 cases with varying s_{max}. The evolution trend is very similar to that of cases A1–A4, except for a more pronounced NED response, i.e. higher peaks of skewness and kurtosis due to higher steepness atop the shoal ε_f and smaller relative water depth μ_f (see table 1).

Combining figures 3 and 4, we conjecture that directional spreading induces only minor changes in the statistical parameters, especially on the top of the bar, where waves are out of equilibrium. The normalised significant wave height ($H_s/H_{s,0}$) is slightly disturbed by the directional spread in the shoaling zone, while it is strongly disturbed in the de-shoaling zone, which is presumably due to wave reflection and refraction. The skewness and the asymmetry parameter are almost unchanged for different s_{max} because of the similar level of wave nonlinearity (steepness) over the bar. Only minor differences are seen over the downslope area, and in the deeper flat region after it. Meanwhile, the net change of kurtosis is mildly reduced for broader directional spreading. In the B4 case with $s_{max} = \infty$ and $\theta_{inc} = 0$, the total kurtosis maximum value achieves 4.61 over the bar, while in the B1 case with $s_{max} = 10$ and $\theta_{inc} = 0$, a comparable value, 4.44 is achieved. Both indicate a strongly non-Gaussian sea state resulting from non-equilibrium wave evolution, and a much higher probability of rogue waves than that expected in a Gaussian sea state.

Figure 5(*a–d*) shows the evolution of statistical parameters for the oblique incident unidirectional wave B4 cases, with $s_{max} = \infty$ and varying θ_{inc}. It is worth mentioning that in panel (*a*), the normalised significant wave height decreases dramatically after the downslope for the case with $\theta_{inc} = \pi/4$. This is due to a limitation of the experimental facility: the wavemaking paddles are installed on one side of the wave tank, thus leaving the last four wave gauges outside the effective experimental zone. Despite the decrease in significant wave height, this case is included for discussion anyway, as the non-Gaussian behaviour on top of the bar is of more interest and is not affected by the facility's limitation. From figure 5(*c–d*), we notice that, not only the maximum values, but also the locations where the maxima of skewness and kurtosis are achieved, vary considerably with θ_{inc}. We attribute this to the effective slope gradient, which is crucial for the wave non-equilibrium evolution. The effective slope, defined as the ratio of the bar height and horizontal upslope length in the direction of wave propagation, reads 1/4.86, 1/5.03, 1/5.61 and 1/6.87 for $\theta_{inc} = 0$, $\pi/12$, $\pi/6$ and $\pi/4$, respectively.

Figure 6(*a*)–(*d*) shows the evolution of statistical parameters in cases that comprise both directionality and oblique incidence. In this case, as the wave fields are of a relatively broad band in directional spreading, wave energy can be transmitted to a broader range in the wave tank; the significant wave height in the case with $\theta_{inc} = \pi/4$ does not reduce as significantly as in figure 5(*a*). The evolution trends of the asymmetry, skewness and kurtosis parameters in figure 6(*b*)–(*d*), are very similar to those observed in figure 5(*b*)–(*d*); their maximum values increase with increasing effective slopes, and the locations where

https://doi.org/10.1017/jfm.2026.11352 Published online by Cambridge University Press

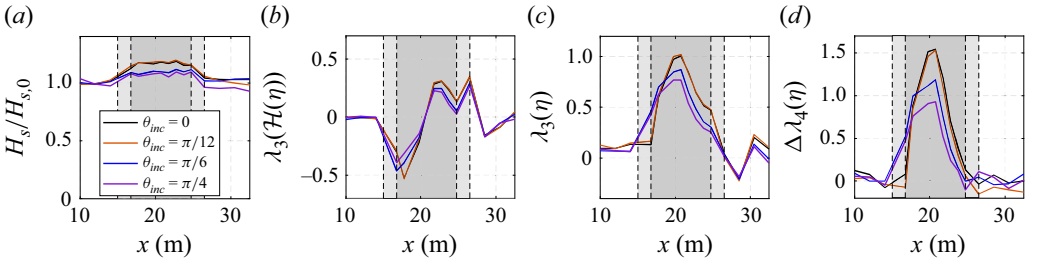


Figure 6. Same as figure 3, but for oblique incident directional cases ($s_{max} = 35$).

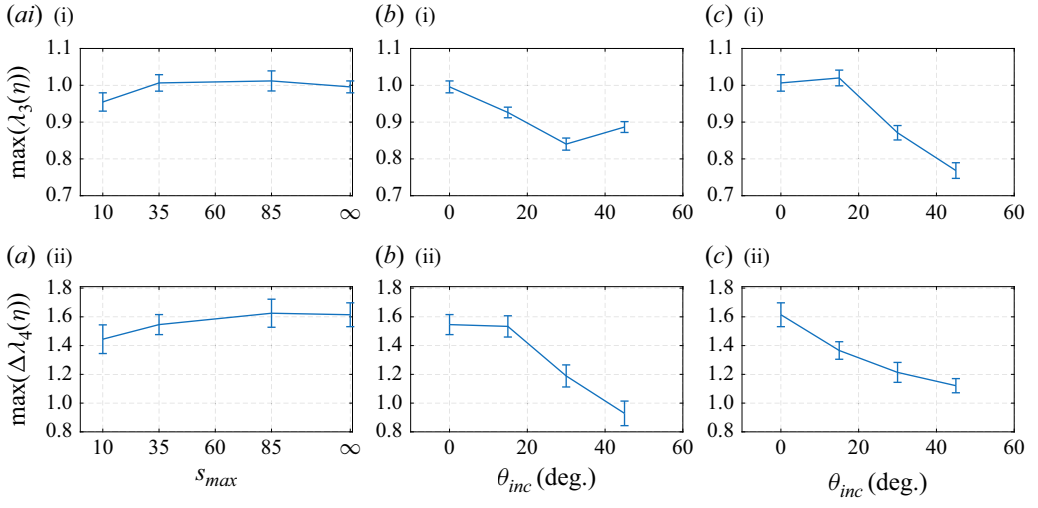


Figure 7. Maximum values of λ_3 and $\Delta\lambda_4$ as functions of θ_{inc} and s_{max}, in normal incident directional wave cases (a), oblique incident unidirectional wave cases (b) and oblique incident directional wave cases with $s_{max} = 35$ (c).

the maxima are achieved shift towards downstream. Inversely, the out-of-equilibrium sea states adapt faster to the new water depth when the effective slope is milder.

To further illustrate the role played by the directionality and the oblique incidence on the non-equilibrium wave dynamics, in figure 7, the maximum values of skewness and kurtosis in the B1–B4 cases are extracted and plotted as functions of s_{max} and θ_{inc}. It is clearly shown in figures 7(a.i) and 7(a.ii) that increasing the directional spreading s_{max} results in only approximately 10 % lower skewness and kurtosis than in the unidirectional case. Our result is in line with the observations of Tang *et al.* (2023), and in contrast to those of Lyu *et al.* (2023). The main reason is that, in the latter work, the relative water depth of the shallower region is around $\mu_f = 1.1$. Although it falls within the typical NED range $0.5 \leq \mu_f \leq 1.3$ (Trulsen *et al.* 2020; Zhang *et al.* 2023), it corresponds to weakly non-equilibrium wave evolution. Thus, the effect of directionality on the non-equilibrium response (e.g. the skewness and net change in kurtosis) is weak and comparable to the statistical error atop the bar, and stronger downslope. In figures 7(b) and 7(c), the effects of oblique incidence, which have been rarely discussed, are shown. We find that the incident angle plays an important role in the magnitude of the non-equilibrium wave response. This is attributed to the effective bottom slope. However, it should be noted that the wave gauge locations were chosen to capture the maximum skewness and kurtosis for the normal

https://doi.org/10.1017/jfm.2026.11352 Published online by Cambridge University Press

incident case, but are likely not optimal for cases with oblique incidence. Therefore, the maximum values of skewness and kurtosis could be underestimated to some extent. Whereas, from the relatively smooth evolution of skewness in figures 5(*c*) and 6(*c*), we believe that the conclusion will not be overturned when the 'actual' maximum values of skewness and kurtosis are considered. Further investigations of oblique incident cases with more wave gauges over the bar, using numerical simulations and statistical distributions, will be discussed in a subsequent paper.

4. Conclusions

The present study provides a comprehensive experimental investigation into the effect of wave directionality on extreme wave formation during nonlinear shoaling, focusing on the NED induced by rapid depth changes. Unlike previous research, which predominantly explored unidirectional irregular waves or directional waves with small directional spread, this work systematically examines multidirectional wave fields using a large-scale wave tank over realistic steep smooth slopes. An oblique incident angle θ_{inc} was chosen up to $\pi/4$ (the limit of our experimental set-up), and a wide range of directional spreadings from $s_{max} = 10$ to a unidirectional condition $s_{max} = \infty$ have been tested. Our results indicate that directional spreading has a minor impact on reducing statistical moments such as skewness and kurtosis for a relatively steep slope, contrasting with previous numerical studies that suggest evident suppression of rogue wave formation due to energy dispersion with directionality.

In contrast to the literature's limited exploration of oblique incidence, the present study highlights the significant role of the incidence direction in NED, driven by the effective bottom slope. This finding extends previous works, which focused on normal incidence, by showing that obliqueness significantly suppresses non-Gaussian behaviour and rogue wave formation. These experimental results, using a Mitsuyasu-type directional spreading function and varying incidence angles, offer a more nuanced understanding than the contradictory numerical simulations, suggesting that future research should prioritise experimental validation and finer resolution studies to clarify this dynamics.

Acknowledgements. The authors wish to acknowledge Dr Z. Guanting from NMEMC and Dr T. Ting from DUT for their technical help during the experimental campaign.

Declaration of interests. The authors report no conflicts of interest.

References

ADCOCK, T.A.A. & TAYLOR, P.H. 2014 The physics of anomalous ('rogue') ocean waves. *Rep. Prog. Phys.* **77**, 105901.

ANNENKOV, S. & SHRIRA, V. 2015 Modelling the impact of squall on wind waves with the generalized kinetic equation. *J. Phys. Oceanogr.* **45**, 807–812.

BENJAMIN, T.B. & FEIR, J.E. 1967 The disintegration of wave trains on deep water. Part 1 theory. *J. Fluid Mech.* **27**, 417–430.

BITNER-GREGERSEN, E.M., GRAMSTAD, O., TRULSEN, K., MAGNUSSON, A.K., STØLE-HENTSCHEL, S., AARNES, O.J. & BREIVIK, Ø. 2024 Rogue waves: results of the ExWaMar project. *Ocean Engng* **292**, 116543.

BOLLES, C.T., SPEER, K. & MOORE, M.N.J. 2019 Anomalous wave statistics induced by abrupt depth change. *Phys. Rev. Fluids* **4**, 011801.

CHIEN, H., KAO, C. & CHUANG, L.Z.H. 2002 On the characteristics of observed coastal freak waves. *Coast. Engng J.* **44**, 301–319.

DEMATTEIS, G., GRAFKE, T., ONORATO, M. & VANDEN-EIJNDEN, E. 2019 Experimental evidence of hydrodynamic instantons: the universal route to rogue waves. *Phys. Rev. X* **9**, 041057.

DIDENKULOVA, E.G., DIDENKULOVA, I. & MEDVEDEV, I. 2023 Freak wave events in 2005–2021: statistics and analysis of favourable wave and wind conditions. *Nat. Hazards Earth Syst. Sci.* **23**, 1653–1663.

https://doi.org/10.1017/jfm.2026.11352 Published online by Cambridge University Press

DIDENKULOVA, E.G. & PELINOVSKY, E.N. 2020 Freak waves in 2011–2018. *Dokl. Earth Sci.* **491**, 187–190.
DRAPER, L. 1964 Freak' ocean waves. *Oceanus* **10**, 13–15.
DRAYCOTT, S. & LI, Y. 2025 Extreme wave amplification through the interplay of wave nonlinearity and a two-dimensional bathymetry. *Phys. Fluids* **37**, 026617.
DUCROZET, G. & GOUIN, M. 2017 Influence of varying bathymetry in rogue wave occurrence within unidirectional and directional sea-states. *J. Ocean Engng Mar. Energy* **3**, 309–324.
DYSTHE, K., KROGSTAD, H.E. & MÜLLER, P. 2008 Oceanic rogue waves. *Annu. Rev. Fluid Mech.* **40**, 287–310.
FEDELE, F., BRENNAN, J., PONCE DE LEÓN, S., DUDLEY, J. & DIAS, F. 2016 Real world ocean rogue waves explained without the modulational instability. *Sci. Rep.* **6**, 27715.
GODA, Y. 2010 *Random Seas and Design of Maritime Structures*. Third edn. World Scientific Publishing Company.
GRAMSTAD, O., ZENG, H., TRULSEN, K. & PEDERSEN, G.K. 2013 Freak waves in weakly nonlinear unidirectional wave trains over a sloping bottom in shallow water. *Phys. Fluids* **25**, 122103.
HE, Y., SLUNYAEV, A., MORI, N. & CHABCHOUB, A. 2022 Experimental evidence of nonlinear focusing in standing water waves. *Phys. Rev. Lett.* **129**, 144502.
KASHIMA, H., HIRAYAMA, K. & MORI, N. 2014 Estimation of freak wave occurrence from deep to shallow water regions. *Coast. Engng Proc.* **1** (34), waves.36.
KHARIF, C., PELINOVSKY, E. & SLUNYAEV, A. 2009 *Rogue Waves in the Ocean*. Springer.
KNOBLER, S., MALILA, M.P., TAYFUN, M.A., LIBERZON, D. & FEDELE, F. 2025 Effects of bound-wave asymmetry on North Sea rogue waves. *Sci. Rep.* **15**, 20609.
LAWRENCE, C., GRAMSTAD, O. & TRULSEN, K. 2021*a* Variational Boussinesq model for kinematics calculation of surface gravity waves over bathymetry. *Wave Motion* **100**, 102665.
LAWRENCE, C., TRULSEN, K. & GRAMSTAD, O. 2021*b* Statistical properties of wave kinematics in long-crested irregular waves propagating over non-uniform bathymetry. *Phys. Fluids* **33**, 046601.
LAWRENCE, C., TRULSEN, K. & GRAMSTAD, O. 2022 Extreme wave statistics of surface elevation and velocity field of gravity waves over a two-dimensional bathymetry. *J. Fluid Mech.* **939**, A41.
LI, Y., DRAYCOTT, S., ADCOCK, T.A.A. & VAN DEN BREMER, T.S. 2021*a* Surface wavepackets subject to an abrupt depth change. Part 2. Experimental analysis. *J. Fluid Mech.* **915**, A72 Part 2.
LI, Y., DRAYCOTT, S., ZHENG, Y., LIN, Z., ADCOCK, T.A.A. & VAN DEN BREMER, T.S. 2021*b* Why rogue waves occur atop a*b*rupt depth transitions. *J. Fluid Mech.* **919**, R5.
LUO, L., LIU, S., LI, J. & JIA, W. 2020 Deterministic reconstruction and reproduction of multi-directional irregular waves based on linear summation model. *Ocean Engng* **198**, 106952.
LYU, Z., MORI, N. & KASHIMA, H. 2023 Freak wave in a two-dimensional directional wavefield with bottom topography change. Part 1. Normal incidence wave. *J. Fluid Mech.* **959**, A19.
MAJDA, A.J., MOORE, M. & QI, D. 2019 Statistical dynamical model to predict extreme events and anomalous features in shallow water waves with abrupt depth change. *Proc. Natl. Acad. Sci.* **116**, 3982–3987.
MAJDA, A.J. & QI, D. 2020 Statistical phase transitions and extreme events in shallow water waves with an abrupt depth change. *J. Stat. Phys.* **179**, 1718–1741.
MEI, L., CHEN, H., YANG, X. & GUI, F. 2023 Statistical properties of extreme waves in multidirectional wave fields over complex bathymetry. *Ocean Dyn.* **73**, 827–849.
MENDES, S. & KASPARIAN, J. 2023 Slope effect on the evolution of kurtosis over a shoal, In *International Conference on Ocean, Offshore and Arctic Engineering*, p. V002T02A017.
MENDES, S., SCOTTI, A., BRUNETTI, M. & KASPARIAN, J. 2022 Non-homogeneous analysis of rogue wave probability evolution over a shoal. *J. Fluid Mech.* **939**, A25.
MENDES, S., TEUTSCH, I. & KASPARIAN, J. 2025 Symmetric influence of forward and opposing tidal currents on rogue wave statistics. *J. Fluid Mech.* **1012**, A22.
MORI, N., WASEDA, T. & CHABCHOUB, A. (Eds) 2023 *Science and Engineering of Freak Waves*. Elsevier.
MOSS, C.S., SCHULTZ, D.M., PARKES, B., LI, Y. & DRAYCOTT, S. 2025 Higher-harmonic contributions to surface elevation, kinematics, and wave loads in wave packets across an abrupt depth transition. *Coast. Engng* **197**, 104693.
NWOGU, O. 1989 Maximum entropy estimation of directional wave spectra from an array of wave probes. *Appl. Ocean Res.* **11**, 176–182.
ONORATO, M., OSBORNE, A.R. & SERIO, M. 2005 Modulational instability and non-Gaussian statistics in experimental random water-wave trains. *Phys. Fluids* **17**, 078101.
ONORATO, M., RESIDORI, S., BORTOLOZZO, U., MONTINA, A. & ARECCHI, F.T. 2013 Rogue waves and their generating mechanisms in different physical contexts. *Phys. Rep.* **528**, 47–89.
ONORATO, M., *et al.* 2009 Statistical properties of directional ocean waves: the role of the modulational instability in the formation of extreme events. *Phys. Rev. Lett.* **102**, 114502.

https://doi.org/10.1017/jfm.2026.11352 Published online by Cambridge University Press

SAMSETH, K. & TRULSEN, K. 2025 Extreme statistics of wave forces on a horizontal cylinder behind a shoal. *J. Fluid Mech.* **1007**, A59.

SHEMER, L., SERGEEVA, A. & LIBERZON, D. 2010 Effect of the initial spectrum on the spatial evolution of statistics of unidirectional nonlinear random waves. *J. Geophys. Res.* **115**, C12039.

TANG, T., BARRATT, D., BINGHAM, H.B., VAN DEN BREMER, T.S. & ADCOCK, T.A.A. 2022 The impact of removing the high-frequency spectral tail on rogue wave statistics. *J. Fluid Mech.* **953**, A9.

TANG, T., MOSS, C., DRAYCOTT, S., BINGHAM, H.B., VAN DEN BREMER, T.S., LI, Y. & ADCOCK, T.A.A. 2023 The influence of directional spreading on rogue waves triggered by abrupt depth transitions. *J. Fluid Mech.* **972**, R2.

TOFFOLI, A., PROMENT, D., SALMAN, H., MONBALIU, J., FRASCOLI, F., DAFILIS, M., STRAMIGNONI, E., FORZA, R., MANFRIN, M. & ONORATO, M. 2017 Wind generated rogue waves in an annular wave flume. *Phys. Rev. Lett.* **118**, 144503.

TRULSEN, K. 2018 Rogue waves in the ocean, the role of modulational instability, and abrupt changes of environmental conditions that can provoke non equilibrium wave dynamics. In *The Ocean in Motion*, pp. 239–247. Springer International Publishing.

TRULSEN, K., RAUSTØL, A., JORDE, S. & RYE, L.B. 2020 Extreme wave statistics of long-crested irregular waves over a shoal. *J. Fluid Mech.* **882**, R2.

TRULSEN, K., ZENG, H. & GRAMSTAD, O. 2012 Laboratory evidence of freak waves provoked by non-uniform bathymetry. *Phys. Fluids* **24**, 097101.

VIOTTI, C. & DIAS, F. 2014 Extreme waves induced by strong depth transitions: fully nonlinear results. *Phys. Fluids* **26**, 051705.

WANG, A., LUDU, A., ZONG, Z., ZOU, L. & PEI, Y. 2020 Experimental study of breathers and rogue waves generated by random waves over non-uniform bathymetry. *Phys. Fluids* **32**, 087109.

ZENG, H. & TRULSEN, K. 2012 Evolution of skewness and kurtosis of weakly nonlinear unidirectional waves over a sloping bottom. *Nat. Hazards Earth Syst. Sci.* **12**, 631–638.

ZHAI, Y., KLAHN, M., ONORATO, M. & FUHRMAN, D.R. 2025 Fully nonlinear simulations of rogue wave formation in finite-depth irregular waves. *J. Fluid Mech.* **1017**, A23.

ZHANG, J., BENOIT, M., KIMMOUN, O., CHABCHOUB, A. & HSU, H.-C. 2019 Statistics of extreme waves in coastal waters: large scale experiments and advanced numerical simulations. *Fluids* **4**, 99.

ZHANG, J., MA, Y. & BENOIT, M. 2024*a* Kinematics of nonlinear waves over variable bathymetry. Part II: statistical distributions of orbital velocities and accelerations in irregular long-crested seas. *Coast. Engng* **193**, 104589.

ZHANG, J., MA, Y. & BENOIT, M. 2024*b* Statistical distributions of free surface elevation and wave height for out-of-equilibrium sea-states provoked by strong depth variations. *Ocean Engng* **293**, 116645.

ZHANG, J., MA, Y., TAN, T., DONG, G. & BENOIT, M. 2023 Enhanced extreme wave statistics of irregular waves due to accelerating following current over a submerged bar. *J. Fluid Mech.* **954**, A50.

ZHANG, J., MENDES, S., BENOIT, M. & KASPARIAN, J. 2024*c* Effect of shoaling length on rogue wave occurrence. *J. Fluid Mech.* **997**, A69.

ZHENG, Y., LIN, Z., LI, Y., ADCOCK, T.A.A., LI, Y. & VAN DEN BREMER, T.S. 2020 Fully nonlinear simulations of unidirectional extreme waves provoked by strong depth transitions: the effect of slope. *Phys. Rev. Fluids* **5**, 064804.

https://doi.org/10.1017/jfm.2026.11352 Published online by Cambridge University Press